Phonon-absorption imaging of the electron-hole liquid in Ge

S. J. Kirch and J. P. Wolfe
Department of Physics, University of Illinois at Urbana—Champaign, 1110 West Green Street, Urbana, Illinois 61801
(Received 4 August 1983)

We report the use of heat pulses to image the spatial distribution of electron-hole liquid (EHL) produced by either cw or pulsed Nd: yttrium aluminum garnet laser excitation. The transmission of phonons through the EHL cloud is observed as the probe pulses are scanned in two dimensions. In contrast to previous phonon-absorption work, the scattering of the fast transverse-acoustic phonons ($\vec{q}||\langle 110\rangle$) is found to be quite strong. For cw clouds 2 mm in diameter, 35% of the probe phonons were scattered or absorbed. For the clouds excited by a high-energy Q-switched pulse, up to 60% of the phonon beam was attenuated. This is nearly all of the phonons which can satisfy energy and momentum conservation, indicating that the pulsed cloud has a much larger filling factor than that of a cw cloud. Interpretation of the large absorption requires the inclusion of hole-phonon scattering, which has not been previously considered. Time-resolved phonon-absorption images show that during the laser pulse the liquid expands at near-sonic velocity. After the pulse, electron-hole droplets are driven for millimeters by the action of a phonon wind, consistent with the results of recent luminescence studies. There is no evidence in the absorption profiles of a large, long-lived source of phonons (Hensel-Dynes hot spot). Additional time- and space-resolved heat-pulse experiments indicate that the long tail ($\tau=5-10$ μsec) in the heat-pulse signal is not due to localized storage of phonons. Instead it is ascribed to elastic and inelastic scattering of the phonons within the bulk of the sample.

I. INTRODUCTION

Much work has been done in the study of photoexcited excitonic states in semiconductors. In Ge, at low temperatures and sufficiently high excitation levels, these carriers condense into a Fermi-fluid phase called the electron-hole liquid (EHL), whose properties are well known.[1] The condensate forms droplets (EHD) of approximately 10^8 pairs and a density, n_0, of 2.4×10^{17} cm^{-3}. Despite their large mass, EHD are observed to move distances of several millimeters into the crystal, forming a cloud with about a 1% filling factor.

This macroscopic transport is due to a phonon-wind force.[2] The nonequilibrium phonons emanating from the excitation region are absorbed by the electrons and holes. The acquired momentum of the individual carrier is rapidly transmitted to the drop as a whole, contributing to its net motion. The phonon flux is anistropic due to phonon focusing.[3] This produces an anisotropic EHL cloud distribution for moderate cw laser powers.[4]

Several authors have examined the EHL phonon scattering directly.[5–9] Phonon pulses were directed through the EHL cloud in various directions. Hensel and Dynes,[6] for example, observed that 35% of longitudinal-acoustic (LA) phonons with $\vec{q}||\langle 111\rangle$ were scattered by a volume-excited cloud. In contrast, they observed[8] only 1—6 % absorption for fast-transverse-acoustic (FTA) phonons with $\vec{q}||\langle 110\rangle$. It seems remarkable that such a weak interaction of FTA phonons with EHL could produce the most prominent features in the cloud—sharp "flares" extending along (100) planes in the crystal.[10] This is an issue which will be addressed in the present paper.

Some experimenters[6,7] used high excitation levels (e.g., from a Q-switched laser) to produce heat pulses for probing the cloud of EHD. In addition, these authors noted that the heat pulses were characterized by a sharp ballistic peak followed by a long tail. To explain this temporal behavior, Hensel and Dynes[6] postulated the existence of a large ($R=600$ μm) long-lived ($\tau=10$ μsec) "hot spot" ($T=8.5$ K) created by the thermalization of the carriers at the excitation surface. It was proposed that phonons within this large hot spot propagate diffusively—with frequent scattering events due to phonon-phonon interactions—but phonons on the edge of the hot spot could travel ballistically to the detector. The principal evidence for this model was the long, power-dependent tail which was observed following the ballistic heat-pulse signals and interpreted as the lifetime of the Hensel-Dynes hot spot.

Using a spatial-filtering technique, Greenstein, Tamor, and Wolfe[11] examined this storage region in some detail. The phonon pulse shapes they obtained were similar to those previously reported,[6,7] but by taking advantage of the phonon-focusing properties of Ge they could separate the localized storage of phonons from the broader background due to bulk scattering. They concluded that the storage region is quite different from the proposed Hensel-Dynes hot spot. It is more localized ($R\leq150$ μm) and has a shorter, power-dependent lifetime ($\tau_s=0.1$ to 1.5 μsec).

In this paper, the phonon-focusing properties of Ge and an unusual sample geometry are utilized to examine both the EHL cloud and the phonons produced by an intense Q-switched laser pulse. By passing a phonon beam

through various parts of the EHL cloud from the side, an "absorption" image of the cloud is formed by the partial shadow it casts. This experiment provides a measure of the absorption length of fast transverse-acoustic (FTA) phonons in the EHD cloud, and gives a means of viewing the rapid cloud-expansion process after an intense laser pulse. Phonon-absorption imaging provides a complementary view of the rapid expansion process which was previously examined by light-scattering[12,13] and luminescence[14,15] techniques.

Briefly it is found that, in contrast to previous phonon-absorption results,[8] up to 35% of the FTA phonons ($\vec{q}||\langle 110\rangle$) are scattered or absorbed by a cw cloud with a diameter of approximately 2 mm. For the case of the Q-switched cloud excitation, up to 60% of these phonons are scattered. The inclusion of isotope scattering is required for the understanding of these large absorption strengths. In fact the 60% absorption is nearly 100% of the phonons which may scatter ($q \lesssim 2k_f^h$), indicating a high average EHL density. Moreover, hole-phonon scattering can no longer be neglected, as indicated also by recent theoretical work.[16] In addition, the time-resolved phonon-absorption images show a rapid "jump out" and a dense expanding shell of liquid, similar to that observed in the luminescence data of Greenstein *et al.*[14] The size of the cloud after jump out is consistent with the formation of a single drop.

Also an attempt is made to directly image the postulated Hensel-Dynes hot spot with probe phonons. Such a strongly diffusive region would be opaque to the probing phonons due to phonon-phonon scattering. We find no resolvable diffusive hot spot, which leads to the conclusion that the phonon storage region must extend less than 150 μm into the sample.

Finally, the origin of the temporally broad heat-pulse signal is examined. When the generation spot is placed "behind" a slot in the sample so that no phonons can propagate directly to the detector, the long tail does not change appreciably. This demonstrates conclusively that the long decay time is not determined by the lifetime of a localized storage region but due to scattering within the bulk of the crystal. A simple model involving only isotope and boundary scattering produces pulse shapes similar to those observed, indicating that a temporally broad signal does not necessarily imply a long-lived source. The model is found to be only qualitatively correct, implying that inelastic scattering is also important.

II. EXPERIMENTAL PROCEDURE

The experimental methods employed here combine the luminescence-imaging[17] and the phonon-imaging[3] techniques. The sample of ultrapure ($N_D - N_A < 10^{12}$ cm^{-3}) Ge, provided by Eugene Haller of Lawrence Berkeley Laboratory, measured $10\times10\times26$ mm^3 and was oriented with the long axis along $\langle 110\rangle$. A slot (0.3 mm wide) was cut approximately halfway through it 3.75 mm from one end. [See Fig. 1(a).] The crystal was etched after all cutting.

The end nearer this slot was coated with a 2000-Å Cu film to provide a phonon emitter surface without photoexcitation of the Ge. A 1500-Å amorphous Ge (α-Ge) film was deposited on top of the Cu film in order to increase optical absorption. A pulsed laser (GaAs or Q-switched Nd:YAG) was used to generate the phonons in these films. The phonons propagated to the other end of the sample where they were detected by an Al bolometer biased at its superconducting transition. A boxcar averager selects the heat-pulse signal at a specified time after the laser pulse. As shown in Fig. 1(b), the position of the phonon-generation spot is scanned by galvo-driven mirrors. Control of these mirrors and storage of the phonon-intensity pattern are accomplished with a microcomputer.

A Nd:YAG laser (cw or Q-switched) was focused in the bottom of the slot to create the EHL cloud. The recombination luminescence was collected through the opposite [110] face and detected by a cooled Ge photodiode. In the case of pulsed EHL excitation, the delay between the two laser pulses could be varied for time resolution of the phonon-absorption image.

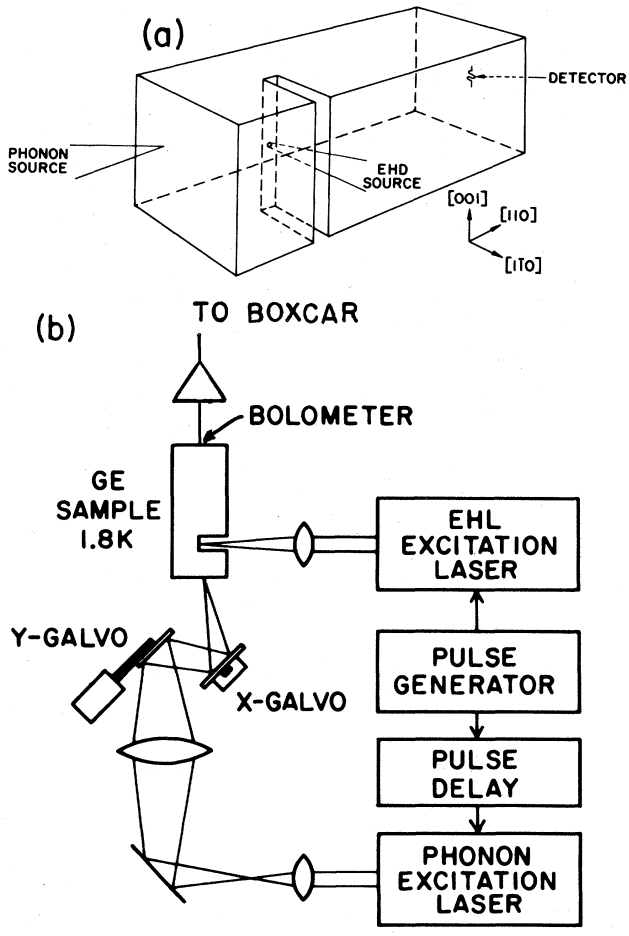

FIG. 1. (a) Schematic of the crystal used. EHL was excited in the bottom of the slot. Phonons were excited in the films on the near end and detected by a serpentine bolometer at the far end. (b) Functional diagram of the experimental setup. The galvo-driven mirrors sweep the phonon-generation spot across the end of the sample to form the image.

III. PHONON-ABSORPTION IMAGING

For the phonon images which follow, the heat pulse was generated by a single-element GaAs laser. The diode was focused to a spot size of 10×400 μm^2 oriented with the long dimension vertical. The pulse was 150 nsec wide with a typical peak power of 600 mW absorbed by the α-Ge film. The bolometer was 150×150 μm^2. The phonon image contains a section of the $\langle 110\rangle$ FTA ridge.[3] The observed signal, shown in Fig. 2(a), ends at the left due to the edge of the sample and at the right due to the presence of the slot.

The boxcar gate delay is fixed to coincide with the peak in the FTA signal. At this low-power level the phonon pulse arriving at the bolometer has approximately the same temporal width as the excitation pulse. The GaAs laser is swept along the center of the intense FTA ridge to produce the slit-scan shown in Fig. 2(b). The sharpness of the cutoff due to the slot corresponds to a spatial resolution of 150 μm.

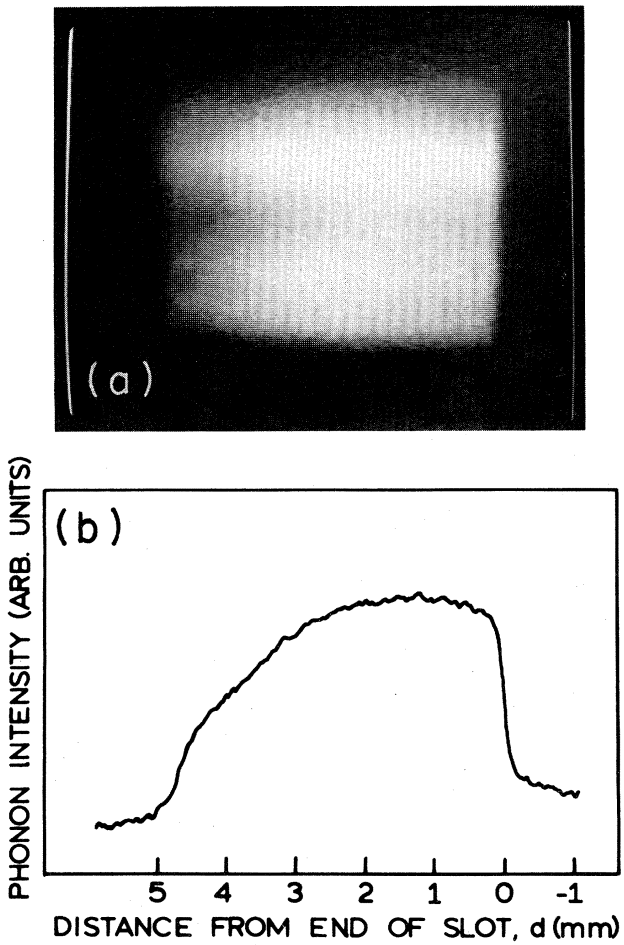

FIG. 2. Phonon signal from the boxcar averager. (a) A two-dimensional phonon image. (b) A slitscan through the center of the image. Distance d is measured from the end of the slot, with negative distance indicating laser positions "behind" the slot, as viewed by the detector.

A. cw cloud excitation

The effect of interposing a cw cloud of EHD between the phonon source and detector is seen in Fig. 3. With no cloud present the slitscan signal [Fig. 3(a)] looks as before. When the laser is incident on the bottom of the slot, it creates free carriers. As these carriers thermalize, they emit phonons (T phonons) some of which impinge on the bolometer. This induces a change in the temperature of the bolometer which alters its sensitivity (by 10—20%) to the heat pulses. The trace of Fig. 3(b) is the bolometer signal in the presence of the cloud, multiplied by a single factor to account for this change in sensitivity. The factor was determined by matching intensity at the left edges of the two slitscans which is unaffected by the presence of the cloud. While the T phonons affect the sensitivity of the detector, this change remains constant as the phonon-generation laser is swept across the metal film. The difference between the cloud-on and cloud-off slitscans is shown in Fig. 3(c). The flatness of the zero demonstrates the accuracy of the normalization procedure. This profile of the EHL cloud agrees well with the known cloud size from previous luminescence results.[17]

As the laser power (EHL cloud size) is varied, the profile changes size in agreement with previous work. The maximum attenuation of these FTA phonons, with $\vec{q}$ approximately along $\langle 110\rangle$, is 35% for a cloud with diameter of about 2 mm. This result seems to contradict the results of a similar experiment by Hensel and Dynes[8] in which they reported attenuations of less than 6% for FTA phonons with $\vec{q}\,||\langle 110\rangle$. In fact for this generation scheme the temperature of the Cu film can be estimated to be 25 K.[18] For this heater temperature, the work of Hensel and Dynes implies that the phonon absorption by EHL

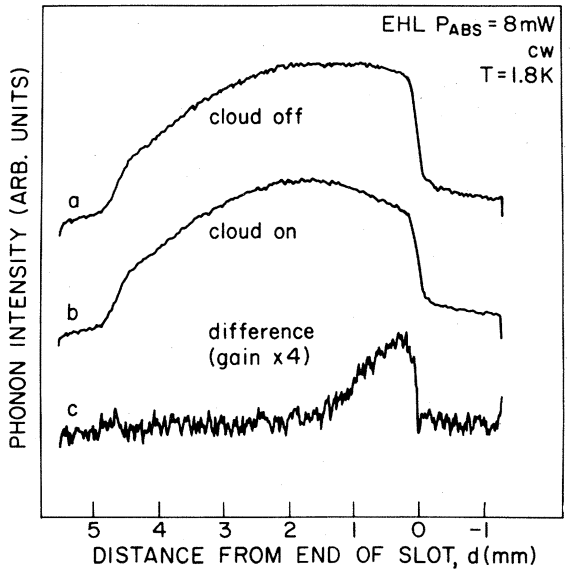

FIG. 3. Effect on a slitscan of an interposed cw cloud. $T=1.8$ K. a: The bolometer signal with no cloud present. b: The bolometer signal with a cw cloud ($P_{abs}=8$ mW) in the phonon beam. This has been normalized so that the phonon intensities at the left edges of a and b match. c: The $4\times$-magnified difference between a and b showing the cloud-absorption profile.

should be less than 1%, making the apparent disagreement even larger. The results can be partially reconciled by examining the effects of isotope scattering and the differing methods of cloud excitation.

For a heater temperature of 25 K, the peak in the Planck energy spectrum is at 1.5 THz. However, the large isotopic impurity of Ge causes the high-frequency phonons to be severely attenuated by the familiar $\tau_i^{-1}=A\omega^4$ where[19] $A=2.88\times10^{-44}$ sec^3. Assuming only isotope scattering, the resultant phonon-frequency distribution which should appear at the detector is shown in Fig. 4. The transmitted intensity peaks at only 200 GHz.

Energy and momentum conservation restrict the electron-phonon scattering to phonons with wave vector q less than twice the Fermi wave vector of the system. This high-frequency ($2k_F$) cutoff was recently observed using phonon spectroscopy.[9] The two vertical lines in Fig. 4 mark the frequencies corresponding to the $2k_F$ cutoffs for the electrons and holes. The phonons are partially absorbed for $q \lesssim 2k_f^h$. One can see that by simply including isotope scattering, it is quite possible to have 35% of the phonons absorbed, depending on the size of the deformation-potential scattering matrix elements and the number of carriers in the phonon path. It is probable that inelastic scattering processes are also present.[11,20] These processes would tend to skew the frequency distribution of the phonons reaching the detector to even lower frequencies. Thus the exact shape of the detected phonon distribution is not known well enough to get a reliable measure of the deformation potentials, but these results indicate that the mean free path for FTA phonons in the (100–300)-GHz range is around 10–50 μm, which is reasonable.[9]

Since Hensel and Dynes[8] used a shorter sample, they detected more phonons with $q>2k_f^h$. Isotope scattering alone, however, cannot reconcile the huge difference between the 1–6% absorption they reported and the 35% measured in this experiment. The majority of the discrepancy may be attributed to the different methods of cloud production. Hensel and Dynes used a lower-power volume pumping at 1.53 μm. The number of electron-hole pairs in the phonon path was no doubt smaller in their case, as evidenced by the smaller cloud diameter they recorded (0.7 mm versus our 2 mm). The phonon absorption by EHD depends also on the average cloud density, and this has not been determined in the volume-pumping case. With regard to cloud size, we find that a reduction by a factor of 2 in radius results in about a factor of 2 smaller absorption, as expected. In conclusion, our results show, that for typical surface-produced cloud sizes and density, a significant fraction of the strongly-focused FTA phonons are absorbed, consistent with the striking features they produce in the cloud.

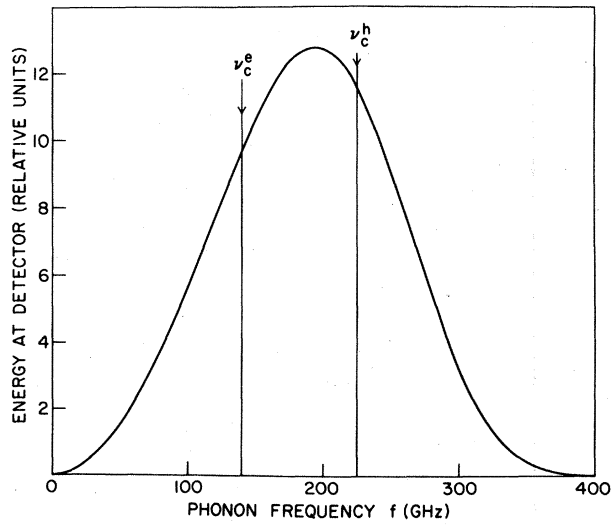

FIG. 4. Predicted FTA phonon intensity arriving ballistically at the detector. A 25-K Planck distribution is attenuated by $e^{-d/l}$ where mean free path, $l=v_s\tau_i$ and $\tau_i^{-1}=(2.88\times10^{-44}$ sec$^3)\,\omega^4$. The two vertical lines indicate the frequencies corresponding to the $2k_F$ cutoffs for electrons ($\nu_c^e=140$ GHz) and holes ($\nu_c^h=225$ GHz).

B. Pulsed cloud excitation

When the cloud is created by a Q-switched Nd:YAG pulse (width 150 nsec), phonon images are obtained as shown in Fig. 5. The time delay between the two laser pulses can be varied and so the cloud profile as a function of time after the creation pulse can be studied. The zero of time corresponds to data taken in which the probe phonons pass by the slot during the EHL excitation pulse. It is important to mention that in this case the effect of the T phonons on the detector is not constant in time. Still their intensity does not vary with the position of the heat-pulse generator. Thus the normalization procedure outlined above should work in this case also.

Figures 5(a) and 5(c) show the phonon images obtained at $t=0$ and 1 μsec, respectively. These images can be normalized in the same way as the slitscans of Fig. 3 and the entire image subtracted from Fig. 2(a). The resultant images are shown in Figs. 5(b) and 5(d). Thus the part of the cloud in the (focused) phonon path can be imaged by this technique. A shell-like structure is observed to move into the crystal with time as was found in luminescence work.[11]

Images were taken for several laser energies at time zero. The size of the cloud was measured by the full width at half maximum (FWHM) of the absorption profile. The cube of the FWHM increased approximately linearly with laser energy. If the number of absorbed photons creates an equal number of electron-hole pairs and are made to fill that measured volume (approximately hemispherical), the average density over the range of energies used was 2.5×10^{17} cm^{-3}, in excellent agreement with the known EHL density. This substantiates the idea that at the end of the laser pulse the carriers have formed a single large drop.

The corresponding slitscan data is displayed in Fig. 6. Both cloud-on and cloud-off data for various times are shown. (Again the cloud-on traces have been multiplied by the appropriate normalization factors.) The resultant subtractions are shown in Fig. 7. Figure 6(a) shows the data for 200 nsec prior to the zero of time. The finite temporal width of the probe and EHL excitation pulses accounts for the slight nonzero difference between the two

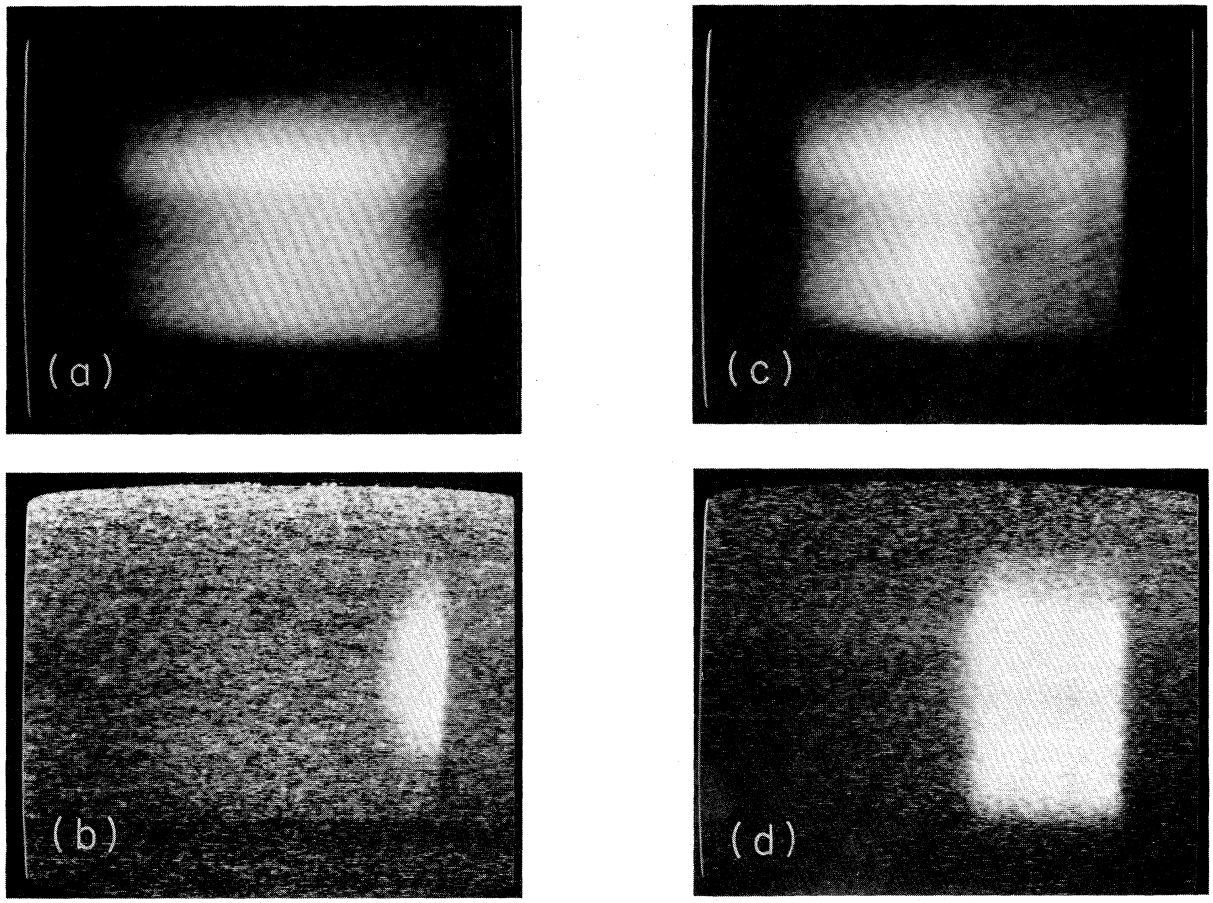

FIG. 5. Phonon images with a Q-switched cloud interposed. $E_{abs}=11$ μJ/pulse. (a) $T=1.8$ K. (b) $t=0$. Image (a) (normalized) subtracted from Fig. 2(a). (c) $t=1.0$ μsec. (d) Image (c) (normalized) subtracted from Fig. 2(a).

curves seen in Fig. 7(a). By $t=0$ [Figs. 6(b) and 7(b)] the half-maximum of the absorption due to the cloud has jumped 0.5 mm into the sample. By only 0.5 μsec later [Figs. 6(c) and 7(c)] the cloud has moved 1.75 mm into the sample. Finally, by 3 μsec [Figs. 6(d) and 7(d)] the cloud has moved only one millimeter further (2.7 mm).

One important thing to notice in Fig. 6 is that for all times and every position at least some of the probe phonons get through the cloud. This is true at all laser powers. If a larger ($R\sim 600$ μm) hot spot were present, the phonon-phonon interaction would effectively block all phonons so a hole would appear in the phonon image the size of this hot region. Thus the storage region must extend less than 150 μm into the sample.

Another interesting fact is available from these data. It is that the electrons cannot be causing all of the phonon scattering. In fact, referring back to Fig. 4, the electrons can only scatter approximately 25% of the phonons (due to the $2k_F$ cutoff). The maximum attenuation of the prompt, ballistic phonons was 60%, which corresponds to nearly all phonons below $2k_F$ for the holes. This implies that the mean free path for phonon-hole scattering (for any phonon in this frequency range) is much less than the diameter of the cloud (1 mm) which attenuates the phonons. In other words the average electron-hole pair density is much higher than it is in a surface excited cloud. This is the first time that the importance of hole-phonon scattering has been isolated from electron-phonon scattering in Ge.

Plots of the width of the cloud profile as a function of time for four different pulse energies are shown in Fig. 8. The solid lines are fits to the theory of Greenstein *et al.* [Eqs. (1) and (2) of Ref. 14]. This theory assumes that the droplets are driven by a disc-shaped source of phonons with a lifetime τ_s. The fitted powers scale quite well with the measured experimental ones. (See Ref. 14 for an explanation.) The source lifetimes do not agree as well with their results. This may be due to the inherent time-resolution limit of phonon-absorption imaging, since the phonon pulse takes a finite time to traverse the photo-excited region. In addition, the surface at the bottom of the slot was not polished prior to etching so the surface quality may be somewhat different than in the sample used by Greenstein *et al.*, which may influence the thermal storage times. Otherwise, this data is in good agreement with that of Greenstein, Tamor, and Wolfe.[14] The initial expansion velocities (after jump out) reach 3×10^5 cm/sec at the highest laser energies.

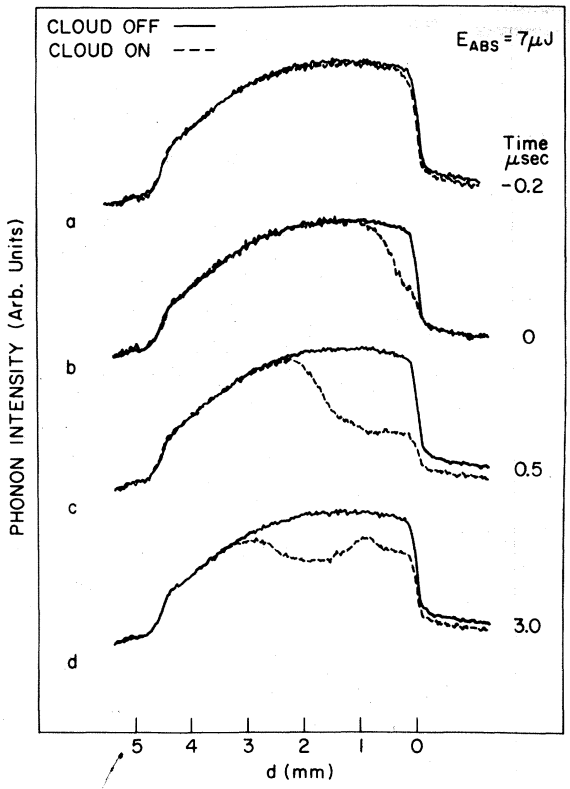

FIG. 6. Slitscans as a function of time after a Q-switched YAG pulse creates the EHL cloud. $E_{abs}=7$ μJ/pulse. $T=1.8$ K. Solid lines are for the cloud absent, and dashed lines indicate the phonon transmission with the cloud present (after normalization). (a) $t=-0.2$ μsec. (b) $t=0$. (c) $t=0.5$ μsec. (d) 3.0 μsec.

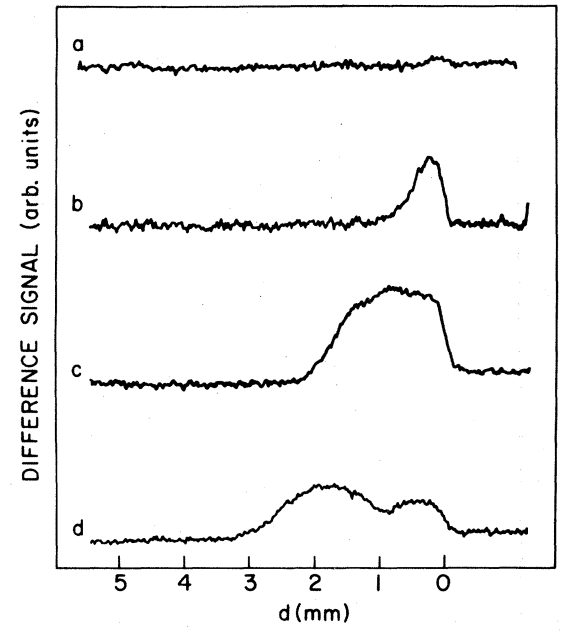

FIG. 7. Cloud profile as given by the difference between the solid and dashed lines of Fig. 6. (a) $t=-0.2$ μsec. (b) $t=0$. (c) $t=0.5$ μsec. (d) $t=3.0$ μsec.

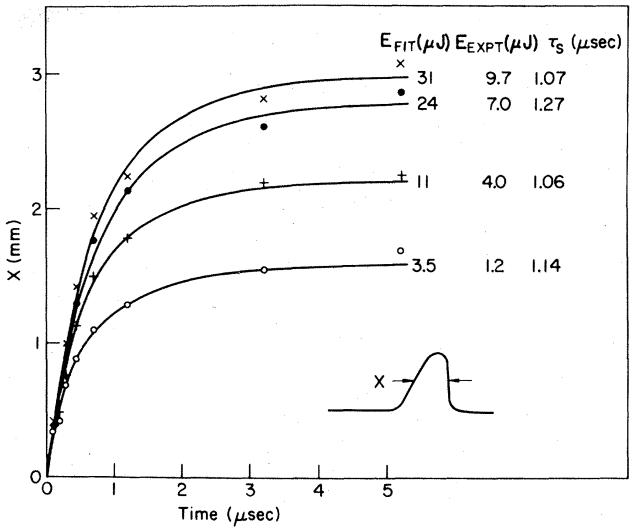

FIG. 8. Full width at half-maximum (see inset) of the cloud profiles as a function of time for four different pulse energies. The lines are fits to the theory of Greenstein, Tamor, and Wolfe (see text).

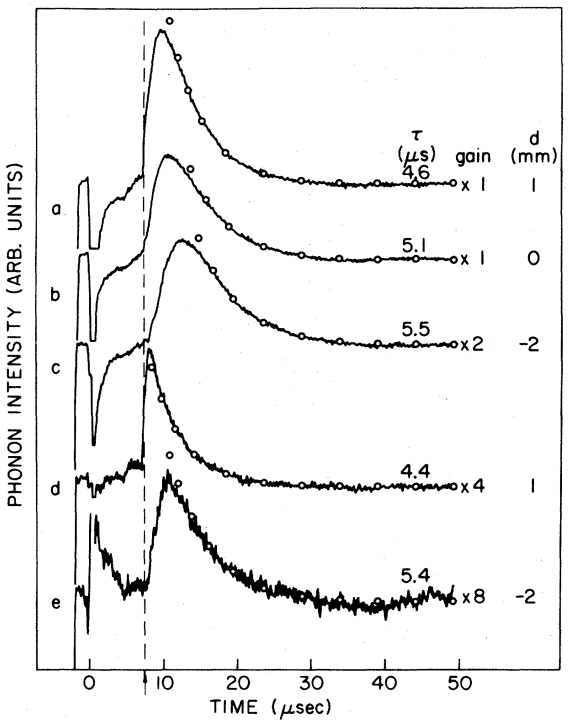

FIG. 9. Phonon signal (from transient recorder/signal averager) as a function of time for various positions (defined in Fig. 2) and laser energies. $T=1.8$ K. The negative spike indicates the photon pulse or $t=0$. The open circles are the fitted decay times. The dashed vertical line represents the ballistic time of flight. (a) $E_{inc}=9.7$ μJ/pulse; $d=1$ mm; (b) $E_{inc}=9.7$ μJ/pulse; $d=0$ mm; (c) $E_{inc}=9.7$ μJ/pulse; $d=-2$ mm; (d) $E_{inc}=1.2$ μJ/pulse; $d=1$ mm; (e) $E_{inc}=1.2$ μJ/pulse; $d=-2$ mm.

IV. TEMPORAL BEHAVIOR OF HEAT PULSES

To directly study the phonons produced by a high-energy laser pulse, the Q-switched Nd:YAG laser was focused to a 100-μm spot on the α-Ge film. (No photoexcitation in the slot). Figure 9 shows the phonon signal as a function of time for such high-energy pulsed conditions. The laser is moved to several points along the FTA ridge and the temporal behavior of the phonon signal is shown for two different laser-pulse energies.

The trace of Fig. 9(a) was made by fixing the laser spot in the center of the FTA ridge approximately 1 mm from the end of the slot. (Distance $d=1$ mm in Fig. 2). The laser intensity was just below the damage threshold ($E_{\text{inc}}=11$ μJ/pulse). Notice the sharp rise due to the onset of the ballistic phonons, the delayed peak, and the long time constant of the tail. These features are similar to those previously reported.[6,7,11] The circles are points from a fitted exponential ($\tau=4.6\pm0.1$ μsec). Figure 9(b) shows the data for the same laser conditions with the laser spot lined up with the end of the slot ($d=0$). Figure 9(c) shows this for 2mm "behind the slot" ($d=-2$ mm), so that no phonon can travel directly from the generation spot to the detector. At first glance, Figs. 9(b) and 9(c) look similar; however, a closer examination shows the leading edge in Fig. 9(c) is shifted to later time. To see this notice that the signal at the ballistic time of flight (dashed vertical line) shrinks dramatically as the generation spot is moved past the edge of the slot, as expected. The peak intensity shifts to a later time as the laser is moved behind the slot and the decay time gradually lengthens [$\tau=5.1$ μsec for Fig. 10(b); $\tau=5.5$ μsec for Fig. 10(c)].

When the pulse energy is reduced by an order of magnitude ($E_{\text{inc}}=1.2$ μJ/pulse), the traces of Figs. 9(d) and 9(e) result. These are the same laser positions as Figs. 9(a) and 9(c), respectively. In comparing traces of different pulse energies obtained at the same generation positions [Fig. 9(a) versus Fig. 9(d) and Fig. 9(c) versus Fig. 9(e)] notice that the position of the peaks in Figs. 9(d) and 9(e) have moved to earlier times but the decay times [$\tau=4.4$ μsec for Fig. 9(d) and $\tau=5.4$ μsec for Fig. 9(e)] are nearly the same as the high-power ones. This indicates that the peak positions are heater-temperature (frequency) dependent but the decay times are not.

Compare the traces with the same pulse energy but different generation spots [Fig. 9(a) versus Fig. 9(c) and Fig. 9(d) versus Fig. 9(e)]. Notice that while the peak positions in the behind-the-slot generation positions have shifted to slightly later times, the pulse shapes have not changed significantly. If the long tail were due to a localized storage of phonons, the signal would disappear entirely when the generation spot is placed behind the slot. Thus the delayed signal cannot be associated with a 600 μm (Hensel-Dynes) hot spot, but must be due to delocalized scattering within the bulk of the crystal.

It is not surprising, then, that the peak in the phonon signals of Fig. 9 change with excitation position and pulse energy. Since phonons which originate at $d=-2$ mm must go "around" the slot, the average number of scatterings for phonons in these heat pulses must be higher. This delays the peak in the phonon signal. Conversely, the phonon signals resulting from lower pulse energies [Figs. 9(d) and 9(e)] have lower initial frequency distributions, implying fewer isotope scatterings and an earlier arrival time, as observed.

In order to examine the effects of various parameters on the pulse shapes, Monte Carlo simulations were used. The model made a number of simplifying assumptions: (i) the crystal is isotropic with a single phonon mode (the velocity corresponds to the FTA mode in Ge, by far the dominant mode which propagates in the $\langle 110\rangle$ direction), (ii) the phonons are generated in the center of one end of a parallelopiped ($10\times10\times25$ mm^3) with a Lambert ($\cos\theta$) distribution, (iii) all isotope scattering events are elastic and randomize the direction of propagation, and (iv) all boundary scattering events are elastic (no mode conversion) and diffusive, again with a Lambert distribution. The mean free path (frequency) for isotope scattering is varied as well as the transmission through the surfaces into the He.

The results for several frequencies and transmission factors are shown in Figs. 10 and 11. The calculations indicate that both phonon frequency and boundary scattering can effectively change the arriving pulse shapes. Still, the exact pulse shapes should not be taken too seriously be-

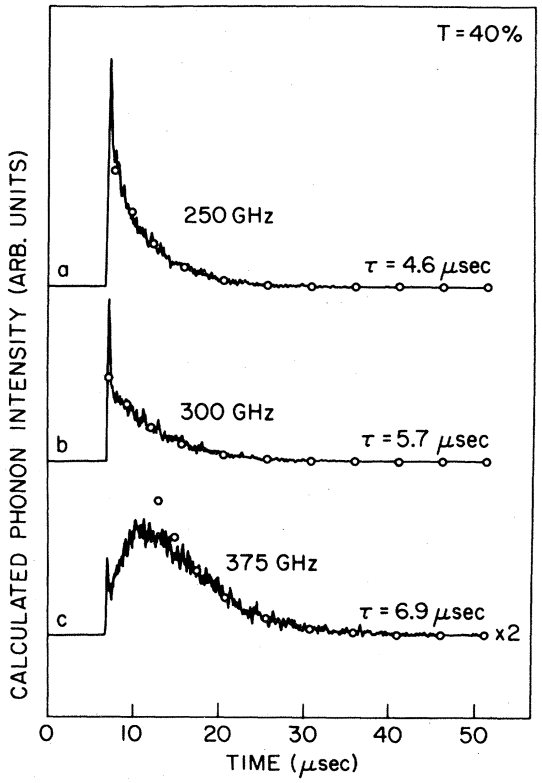

FIG. 10. Results of the Monte Carlo simulation: predicted phonon intensity as a function of time for three frequencies or mean free paths, l, assuming no frequency downconversion. The open circles represent fits to the signal decay times, τ. The calculation assumes that 40% of the phonons which encountered a crystal boundary were transmitted into the helium bath. (a) $\nu=250$ GHz; ($l=2.5$ cm). (b) $\nu=300$ GHz; ($l=1$ cm). (c) $\nu=375$ GHz; ($l=0.5$ cm).

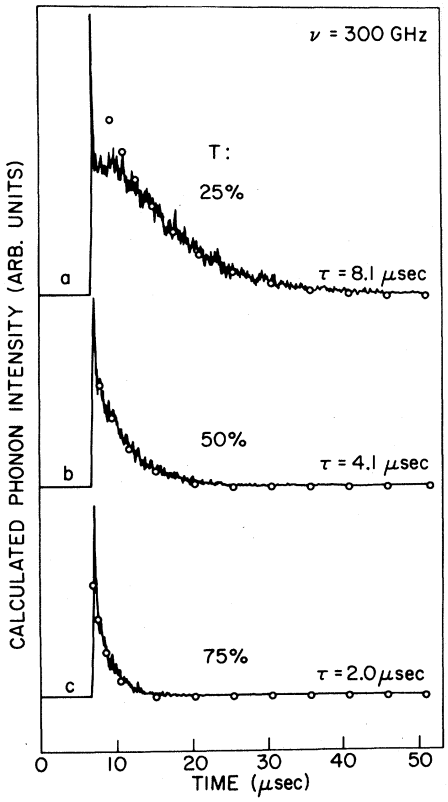

FIG. 11. Results of the Monte Carlo simulation: predicted phonon intensity as a function of time for various probabilities of transmission into the helium bath, T. Again, the open circles represent fits to the decay times. $\nu=300$ GHz, $l=1$ cm. (a) $T=25\%$. (b) $T=50\%$. (c) $T=75\%$.

cause of the approximations stated above and the omission of inelastic processes in the calculation. Previous work[20] has indicated the importance of such processes. The effect of surface transmission seems to be exaggerated in the calculations. A subsequent experiment using a $10\times10\times5$-mm sample of ultrapure Ge (the short dimension was the $\langle 110\rangle$ propagation direction) showed a reduction of only 15% in the decay time in the long tail compared to the longer sample. Still, it is seen that broad pulses of the order of the experimentally measured widths are produced by assuming accepted values for bulk scattering, and hence no long-lived hot spot is necessary to explain the data.

V. CONCLUSION

Phonon-absorption imaging has been used to study EHL cloud distributions for both cw and pulsed-excitation conditions. For the cw cloud, up to 35% of the FTA phonons were absorbed, explaining the prominent features in the cloud. For pulsed excitation, up to 60% absorption was observed, even though the initial plasma volume was an order of magnitude smaller than that of the cw cloud. Assuming the simple isotope scattering calculation presented here, this large absorption implies that nearly all of the phonons with wave vectors below $2k_f^h$ are absorbed. Thus, the liquid initially formed by the high-intensity 150-nsec pulse has a much greater *average* density than the cw-produced cloud. The results of these studies support the idea that initially the EHL created by a high-energy laser pulse forms a single drop as suggested by Greenstein, Tamor, and Wolfe.[14] In order to distinguish between the plasma-expansion idea of Combescot[21] and the growth of a constant-density single drop of EHL,[15] better time resolution is required. Following this initial jump-out process, the EHL distribution expands at subsonic velocities for several microseconds, indicating a persistent phonon-wind source. Further it is concluded that both holes and electrons effectively scatter the probe phonons. If a phonon spectroscopy technique were employed, the deformation potentials for holes could be directly measured.

For high-energy pulses the presence of a large ($R\sim600$ μm), long-lived ($\tau=10$ μsec) hot spot was not observed. Instead, the thermal storage region is much smaller, less than 150 μm thick, and has a lifetime of up to 1.5 μsec, which is considerably shorter than the heat-pulse tail. The temporally broad part of the heat-pulse signal remained substantially unchanged when the ballistic path between generation spot and detector was completely blocked, showing that this tail is due to scattering within the bulk of the crystal. A complete description of this phenomenon must include inelastic decay processes as well as isotope and boundary scattering.

ACKNOWLEDGMENTS

The authors would like to thank M. Greenstein and G. Northrop for their many helpful discussions. This work was supported by National Science Foundation Grant No. NSF-DMR-80-24000 with facility support provided by Grant No. NSF-DMR-80-20250.

[1]See, for example, reviews by J. C. Hensel, T. G. Phillips, G. A. Thomas, and T. M. Rice, *Solid State Physics,* edited by H. Ehrenreich, F. Seitz, and D. Turnbull (Academic, New York, 1977), Vol. 32.

[2]L. V. Keldysh, Zh. Eksp. Teor. Fiz. Pis'ma Red. 23, 100 (1976) [JETP Lett. 23, 86 (1976)].

[3]G. A. Northrop and J. P. Wolfe, Phys. Rev. B 22, 6196 (1980).

[4]R. S. Markiewicz, M. Greenstein, and J. P. Wolfe, Solid State Commun. 35, 339 (1980).

[5]V. S. Bagaev, L. V. Keldysh, N. N. Sibel'din, and V. A. Tsvetkov, Zh. Eksp. Teor. Fiz. 70, 102 (1976) [Sov. Phys. JETP 43, 362 (1976)].

[6]J. C. Hensel and R. C. Dynes, Phys. Rev. Lett. 39, 969 (1977).

[7]V. S. Bagaev, G. Bel'skaya-Levandovskaya, M. M. Bonch-Osmolovskii, T. I. Galkina, S. Yu. Levandovskii, G. N. Mikhailova, A. G. Poyarkov, and G. Jung, Zh. Eksp. Teor. Fiz. 77, 2117 (1979) [Sov. Phys.—JETP 50, 1013 (1979)].

[8]J. C. Hensel and R. C. Dynes, *Physics of Semiconductors,* edited by B. H. L. Wilson (Institute of Physics, London, 1979), p. 371; *Phonon Scattering in Condensed Matter,* edited by H. J.

Maris (Plenum, New York, 1979), p. 395.
[9]W. Dietsche, S. J. Kirch, and J. P. Wolfe, Phys. Rev. B 26, 780 (1982).
[10]J. P. Wolfe, M. Greenstein, and G. A. Northrop, J. Phys. Soc. Jpn. 49, Suppl. A 491 (1980).
[11]M. Greenstein, M. A. Tamor, and J. P. Wolfe, Phys. Rev. B 26, 5604 (1982).
[12]T. C. Damen and J. M. Worlock, *Proceedings of the Third International Conference on Light Scattering in Solids, Campinas, Brazil, 1975* (Flammarion, Paris, 1976), p. 183.
[13]N. V. Zamkovets, N. N. Sibel'din, V. B. Stopachinskii, and V. A. Tsvetkov, Zh. Eksp. Teor. Fiz. 74, 1147 (1978) [Sov. Phys. JETP 47, 603 (1978)].
[14]M. Greenstein, M. A. Tamor, and J. P. Wolfe, Solid State Commun. 45, 355 (1983).
[15]M. Tamor, M. Greenstein, and J. P. Wolfe, Phys. Rev. B 27, 7353 (1983).
[16]M. Uwaha and G. A. Baym (unpublished).
[17]M. Greenstein and J. P. Wolfe, Phys. Rev. B 24, 3318 (1981).
[18]O. Weis, J. Phys. (Paris) C4, 49 (1972).
[19]For a brief discussion of an experimental measurement of A, see P. G. Klemens, in *Solid State Physics,* edited by H. Ehrenreich, F. Seitz, and D. Turnbull (Academic, New York, 1958), Vol. 7, pp. 59—64.
[20]R. E. Horstman and J. Wolter, Phys. Lett. 85A, 369 (1981).
[21]A theoretical model is provided by M. Combescot, Phys. Rev. B 12, 1591 (1975).

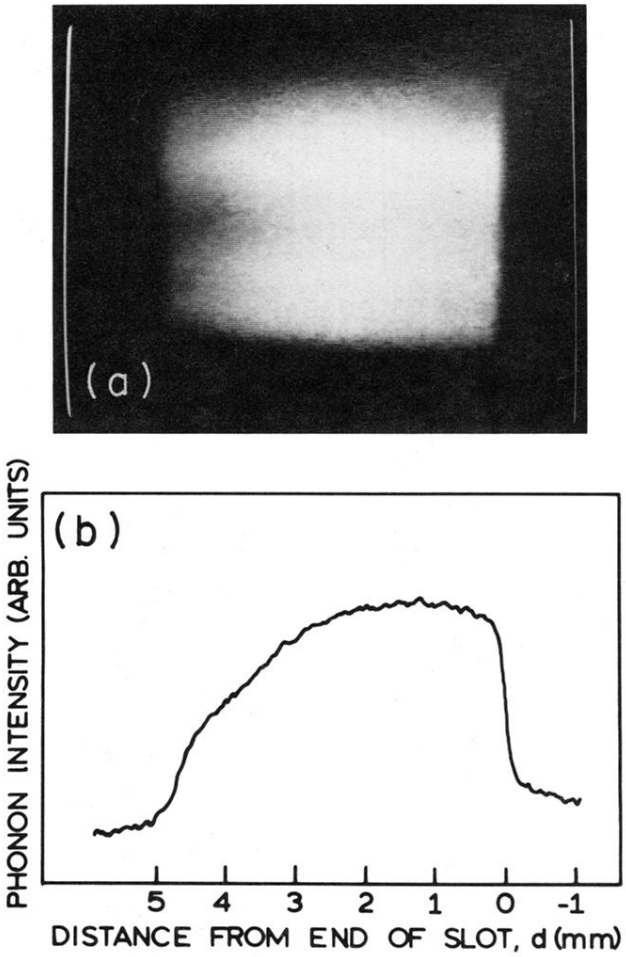

FIG. 2. Phonon signal from the boxcar averager. (a) A two-dimensional phonon image. (b) A slitscan through the center of the image. Distance d is measured from the end of the slot, with negative distance indicating laser positions "behind" the slot, as viewed by the detector.

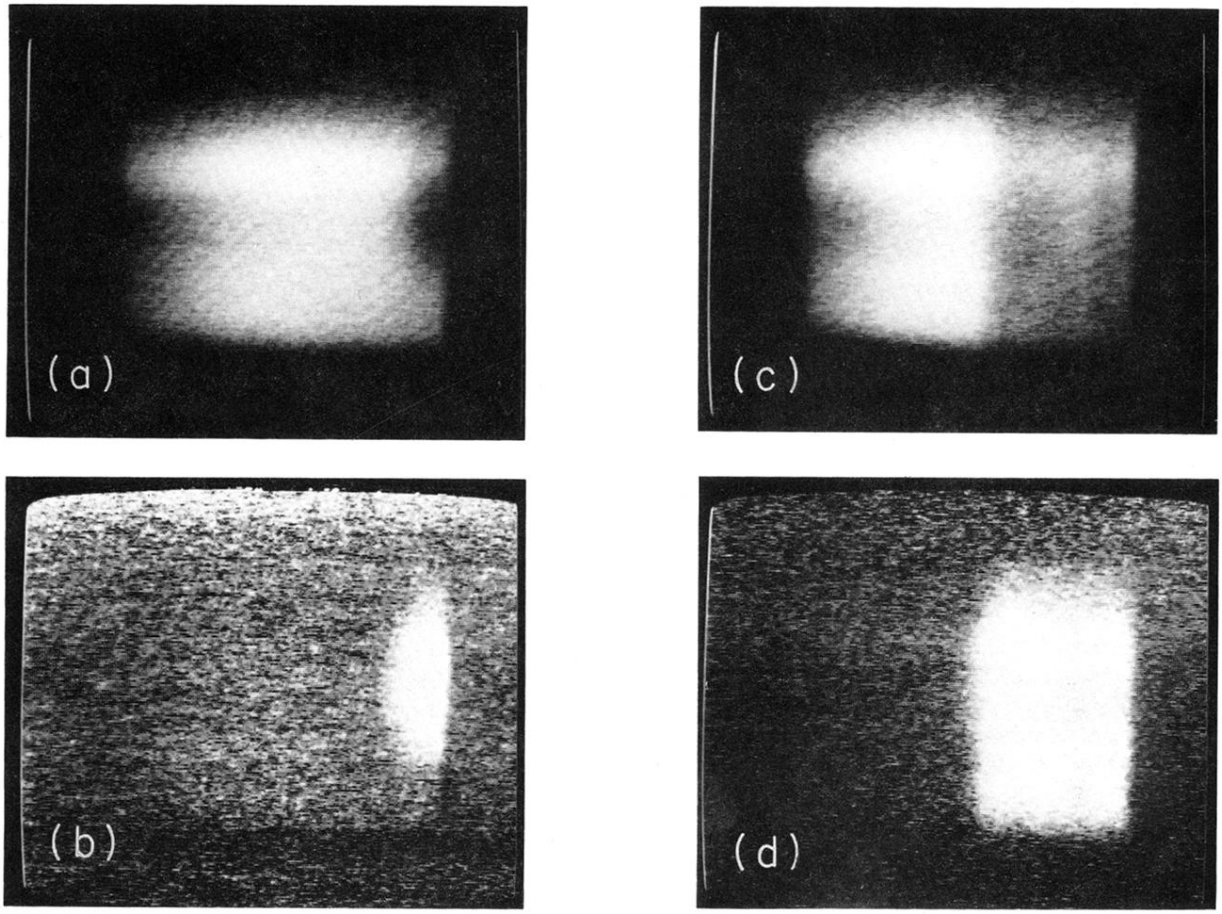

FIG. 5. Phonon images with a Q-switched cloud interposed. $E_{abs}=11\ \mu J$/pulse. (a) $T=1.8$ K. (b) $t=0$. Image (a) (normalized) subtracted from Fig. 2(a). (c) $t=1.0\ \mu$sec. (d) Image (c) (normalized) subtracted from Fig. 2(a).